SAR DOPPLER CALIBRATION AND APPLICATION FOR SEA ICE DRIFT ESTIMATION

Jeong-Won Park[1], Morten Hansen[2], Anton Korosov[2], Hyun-Cheol Kim[1]

[1]Korea Polar Research Institute, Incheon, South Korea
[2]Nansen Environmental and Remote Sensing Center, Bergen, Norway

ABSTRACT

We propose a Doppler calibration scheme that effectively removes errors come from attitude anomaly and antenna mispointing which are generic for all SAR sensors. The resulting calibrated Doppler signal of the entire ENVISAT ASAR ScanSAR data for one repeat cycle (35 days) showed well-balanced inter-swath measurements and largely reduced uncertainty without relying on bias correction using land reference. Sea ice drift in the Fram Strait was derived using both the offset-tracking and the Doppler estimation. An inter-comparison of the time-averaged velocities showed overall high consistency with RMSE of 0.15 m/s.

Index Terms— Synthetic aperture radar, Doppler, sea ice, velocity estimation, ENVISAT ASAR

1. INTRODUCTION

SAR Doppler is a unique application that can extract instantaneous velocity field at no extra cost in all kinds of existing SAR system. The applications were mainly ocean wind and/or surface current retrieval [1] and ground moving target indication [2], and recently the Doppler measurements were tested for retrieving sea ice drift field [3,6].

The main challenges for extending Doppler application to sea ice motion are the low speed of the sea ice drift, which ranges 2-23 cm/s in the Fram Strait [4], and several uncertainties in the Doppler estimation procedure. Regarding the former issue, the measurement precision must be higher than the expected Doppler shift caused by the target's motion along the line-of-sight (LOS) direction. In terms of Doppler frequency, an error of 1 Hz would translate to an error in the ground velocity of 5.6 cm/s at 30° incidence angle using ENVISAT ASAR system, thus the accuracy of the absolute Doppler should be better than 2 Hz to capture the ice drift moving in a moderate speed. However, it should be noted that the instantaneous speed can be higher than the known averaged speed considering typical non-linearity of the sea ice drift. The latter issue is related to the system and processing related calibration. Previous study was only able to suppress the measurement uncertainty down to 5 Hz [3,5], which is not enough for sea ice application. If possible, the Doppler processor must be calibrated precisely so that the uncertainty does not exceed the lower limit for sea ice application (i.e., 2 Hz). Recent study in [6] demonstrated the first quantitative comparison between ice drift derived from the Doppler shift and image pair with a short time lag of 25 minutes, however, the tested image was only a single scene and the applied Doppler calibration was not generic, thus the results cannot be generalized.

In this study, we examine an extensive set of ENVISAT ASAR ScanSAR data to improve the Doppler calibration, and then evaluate the feasibility of extending Doppler measurement for retrieving sea ice motion field with combined use of the image offset-tracking based drift estimation [7].

2. DOPPLER CALIBRATION

The Doppler centroid shift measurement from any SAR sensor must be calibrated for non-geophysical biases. We follow the approach described in [5] with several improvements that make the calibration more precise. The raw Doppler centroid can be modelled as follows:

$$f_{DC} = f_{geom} + f_{em} + f_{geop} \quad (1)$$

where f_{geom} is the geometric Doppler which is related to the relative motion between the SAR antenna and the rotating Earth surface, f_{em} is the electronic mispointing originated by misalignment and failure of antenna transmit/receive module, and f_{geop} is the geophysical Doppler induced by true motion of the target. The raw Doppler centroid, f_{DC}, was calculated using NORUT GSAR processor which supports full azimuth band SAR focusing and side-band correction [8]. Doppler calibration is a procedure that eliminates non-geophysical terms, f_{geom} and f_{em}, from f_{DC}.

For establishing and validating calibration parameters, we collected the entire ENVISAT ASAR ScanSAR mode data acquired for one full repeat cycle (35 days) from January 1 to February 4, 2010. The number of processed strips were 1328 for HH polarization.

2.1. Geometric Doppler

The geometric Doppler can be calculated by solving the range-Doppler equations as described in [9]. For ENVISAT ASAR, key parameters like yaw and pitch steering law, orbital state vectors, and attitude vectors are available with high precision so that the uncertainty is expected to be

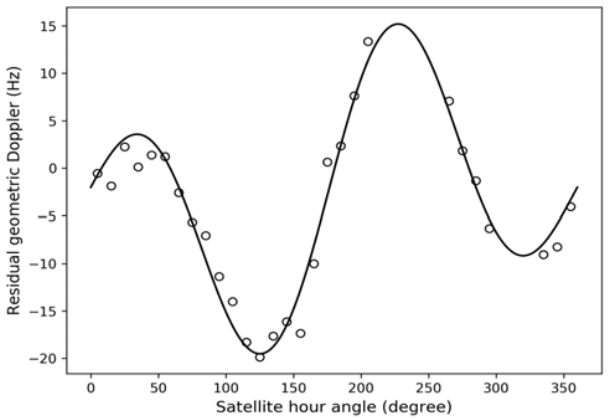

Fig. 1. Estimated residual Doppler drift after compensating for geometric Doppler. Solid line represents a best-fit curve. The RMSE of the fit is 1.8 Hz.

sufficiently low. However, even small amount of antenna misalignment along satellite body axes can make a significant Doppler offset as reported in [10]. Considering any unexpected/untracked attitude anomalies along the orbits during the mission, this misalignment contribution must be estimated from the data by comparing estimated Doppler centroid with predicted Doppler centroid over land coverage. This can be done by removing the linear trend and offset from the residual Doppler after subtracting the initial geometric Doppler computed without considering any misalignment angles. The derived misalignment was 0.209° and 0.026° in yaw and pitch angle, respectively. These numbers are similar to the those in [10], which are 0.21° and 0.02°.

After removing f_{geom} from f_{DC}, there were residual Doppler shifts that changes with the satellite hour angle (or satellite osculating true latitude). Fig. 1 shows the estimations and their best fit curve. The pattern is similar to the typical geometric Doppler itself, however the amplitude is much lower, and the sign is opposite. The residual Doppler shifts, f'_{geom}, can be modeled by curve fitting using a slightly modified version of the ENVISAT's steering law in [11]:

$$f'_{geom} = [\,-7.8\,\times \sin(\gamma_h + 0.12) - 224.8\,] + [\,11.5\,\times \sin(2\gamma_h - 0.12) + 222.4\,] \quad (2)$$

where γ_h is the satellite hour angle. Since the best fit curve followed the estimation with RMSE of 1.8 Hz, the geometric Doppler correction combined with the residual drift correction using (2) can be considered qualified for estimating small changes in Doppler shift at such level.

Antenna look angle is also an important information that must be calculated precisely during the geometric Doppler computation, and is stored for retrieving Doppler mispointing in the next subsection. Topographic height change causes not only small Doppler shift but also look angle shift which is particularly sensitive when estimating the antenna mispointing from real data. For example, 1 km of height

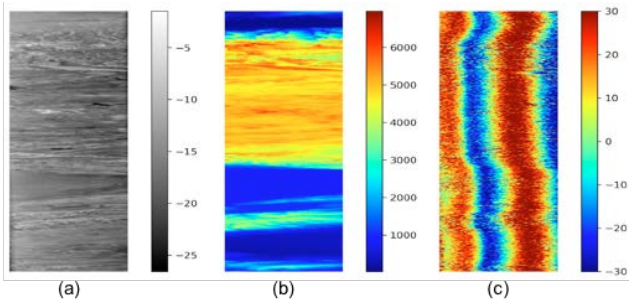

Fig. 2. An extreme case showing the correlation between topographic height and electronic mispointing. (a) sigma naught, (b) radar-coded topographic height, (c) Doppler frequency corrected for geometric Doppler.

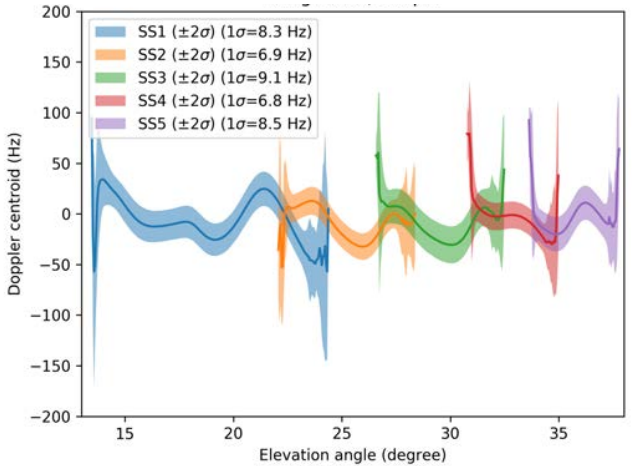

Fig. 3. Estimated Doppler frequency anomaly caused by electronic antenna mispointing.

difference at 25° off-nadir angle induces 2.7 Hz of geometric Doppler and 0.13 degree of look angle.

2.2. Electronic mispointing

The electronic mispointing can be derived either from an antenna model or directly from the observed SAR data. The former requires several parameters that are not publicly available, and the error is up to 5 Hz [12], which translates to a velocity difference of 28 cm/s at 30°. Considering the range of typical sea ice drift speed, this amount of error is too large for practical application.

Since the electronic mispointing is a function of antenna look angle, a look-up table can be made from extensive Doppler measurements over land pixels by taking the mean Doppler anomaly corrected for the geometric Doppler (i.e. $f_{DC} - f_{geom}$) at each of the look angle bins. However, the number of samples should be large, and the geographic and geometric distribution should be diverse in order to make a reliable look-up table. Fig. 2 shows an extreme case of look angle changes by topographic heights in a single scene. Clearly the Doppler shift induced by electronic mispointing is not consistent at each range bin, and the shift is correlated with topographic height. After calculating correct look angles for land pixels from many strips, a look-up table for electronic

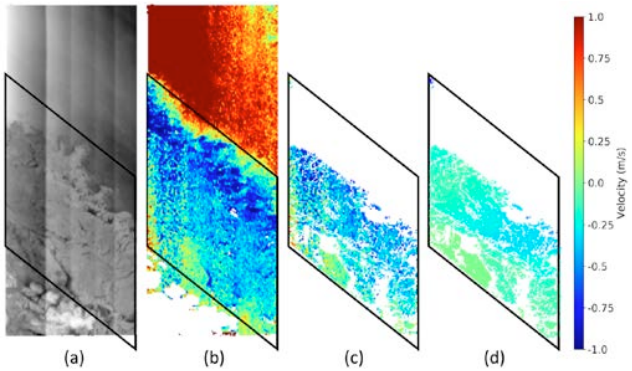

Fig. 4. Comparison of the SAR Doppler derived instantaneous velocity and the offset-tracking based mean velocity. (a) backscattering intensity, (b) Doppler derived instantaneous velocity, (c) masked version of (b) using the valid points in (d) offset-tracking derived mean velocity.

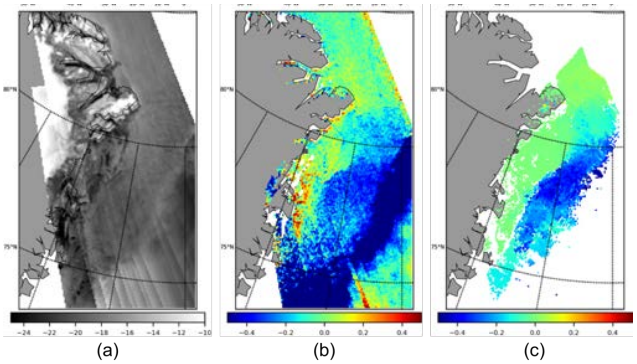

Fig. 5. Comparison of time-averaged (35 days) velocity fields from (b) SAR Doppler estimation and (c) offset-tracking.

mispointing can be made by taking median values of Doppler frequency for each look angle bins.

Fig. 3 represents the Doppler mispointing of all five subswaths (SS1-SS5) for HH polarization channel. The overlapped area between the subswaths exist because of the changes in the effective antenna elevation angle for given topographic heights. The sigma RMSEs for each of the subswaths are around 8 Hz, which is lager than those from the antenna model-based estimations in [12]. However, the values reported in [12] were evaluated using a single image over a rainforest area where the signal-to-noise ratio is known to be very high, while our measurements were done over the entire solid earth surface with various surface types. Thus, our estimation can be representative for practical cases. Although the error levels are higher than the requirements of 2 Hz, the estimation errors can be reduced by ensemble averaging over time and space. The actual performance of the stacking approach will be discussed in the next section.

Once a look-up table is generated, it can be used to compensate for Doppler mispointing from any images. This is particularly important for images acquired over sea ice where typically no nearby land reference is available for bias correction.

3. SEA ICE DRIFT ESTIMATION

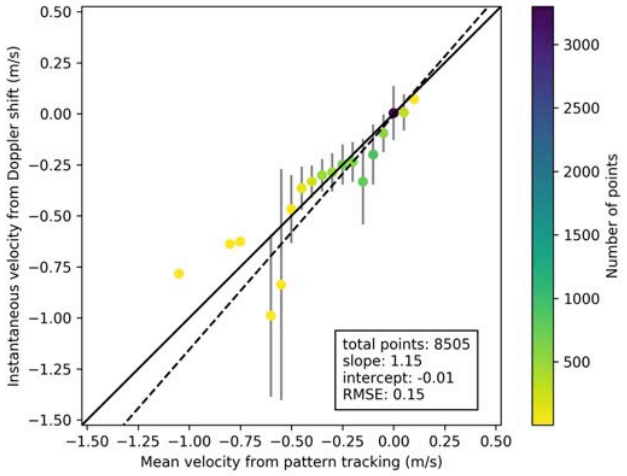

Fig. 6. Scatter plot for the estimations in Fig. 5.

Among the collected ScanSAR strips over the Fram Strait, we applied the developed Doppler calibration scheme for image strips over the north-east Greenland Sea where the sea ice motions are relatively fast. Considering the acquisition geometry, we selected images from the ascending path only. From the offset-tracking based drift estimation, the range direction component was used for intercomparing with the Doppler based drift estimation results.

Fig. 4 shows an example of the Doppler-derived instantaneous velocity field and its corresponding offset-tracking-derived mean velocity field for a single image acquired on January 26, 2010. The SAR Doppler based velocity (Fig. 4(b)) was available for almost every pixels in the image while the offset-tracking based velocity (Fig. 4(d)) was available only where distinct feature/pattern exists. The overall velocity directions and magnitudes match well, while the instantaneous velocity can be different from the mean velocity, thus motion vectors are different locally. Note that the overall measurements from Doppler looks noisier.

In order to evaluate the similarity between the two velocities from two different methods, time averaged data were compared. We selected 10 image strips over nearly the same area and averaged the derived velocities. Fig. 5 shows the averaged results for the Doppler-derived velocity and the offset-tracking-derived velocity. The ice-water boundary can be recognized from the backscattering image and the Doppler-derived velocity map while it is not from the offset-tracking-derived velocity map. This indicates a potential use of Doppler for investigating marginal ice zone where the ice motion is different from typical large ice floes. The sharp boundaries between non-moving fast ice and drifting ice are clearly seen in both results. A quantitative comparison between the two velocity fields is shown as one-to-one scatter plot in the Fig. 6. The slope was 1.15, which indicates the instantaneous velocity was 15% faster than the mean velocity, however, this changes from scene to scene as the actual short-term motion of sea ice is highly heterogeneous. Intercept and RMSE are more important parameters here,

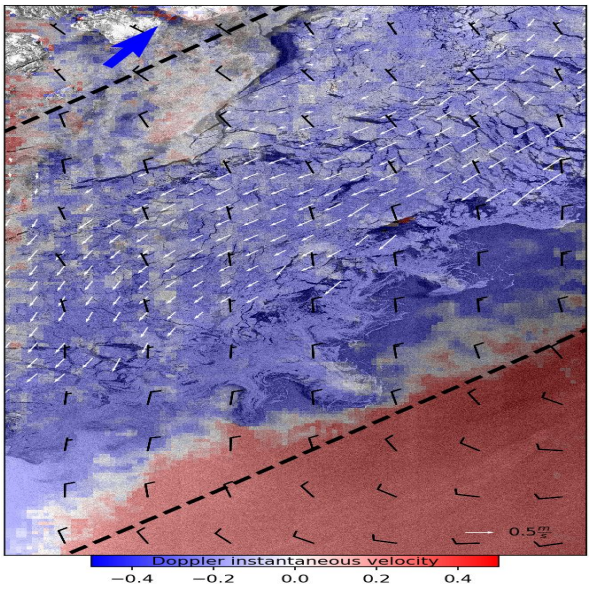

Fig. 7. Ice drift in the Fram strait.

since they tell how the two genuinely different velocity are related. The intercept was only -0.01 m/s, which means the two time-averaged velocity fields have negligible difference in their mean. The RMSE of 0.15 m/s indicates how the two velocities disagree in time series.

4. DISCUSSION AND CONCLUSIONS

Because of several uncertainties in the Doppler estimation procedure, the resulting sea ice drift product has generally rather high noise and low sensitivity to the motion of sea ice. Nonetheless, the Doppler algorithm has a great advantage: it provides the range component of ice drift speed in the marginal ice zone and deformation zones where offset-tracking does not work. By filling the gaps and extrapolating ice drift field it helps qualitative analysis and understanding the processes of ice/ocean/atmosphere interaction on the case-by-case basis. Fig. 7 illustrates the advantage of combining offset-tracking (shown as white arrows) with Doppler (shown as blue/red hue) and with auxiliary products (wind speed and direction is shown by wind barbs; SAR image is in the background). Thick dashed lines show boundaries of the second SAR scene taken from descending orbit along the sea ice flow and used for the offset-tracking. Blue arrow shows the North direction.

There are two key findings that we got from this study:

i) Doppler calibration is crucial for identifying relatively slow-moving geophysical phenomenon like sea ice drift. Considering the sensitivity of Doppler shift to actual motion in LOS direction, the signal uncertainty must be lower than 2-3 Hz. The proposed calibration scheme effectively removes errors comes from attitude anomaly and antenna mispointing which are generic for all SAR sensors including Sentinel-1. The resulting calibrated Doppler signal showed largely reduced uncertainty (RMSE: 1.8 Hz for geometric Doppler correction; 8 Hz for electronic mispointing bias correction) and well-balanced inter-swath measurements. The Doppler calibration has an advantage in universal Doppler observation capability regardless land correction which has been considered crucial for Doppler calibration of individual scenes.

ii) Despite the low signal-to-noise ratio, low efficient resolution and only one component of the drift vector, the Doppler algorithm proves to be very useful for complementing the offset-tracking algorithm in the MIZ and ice deformation zones. An approach for assimilation of the Doppler instantaneous velocity into mean ice drift speed is proposed and its efficiency is illustrated in a case study.

ACKNOWLEDGEMENT

This work was supported by the ESA funded PRODEX DESIce project (Contract No. 4000115940) and PRODEX ISAR project (Contract No. 4000108820)

REFERENCES

[1] B. Chapron, F. Collard, and F. Ardhuin, "Direct measurements of ocean surface velocity from space: Interpretation and validation," *J. Geophys. Res.*, vol. 110, no. C7, pp. 1–17, Jul. 2005.

[2] J.-W. Park and J.-S. Won, "An efficient method of Doppler parameter estimation in the time–frequency domain for a moving object from TerraSAR-X data," *IEEE Trans. Geosci. Remote Sens.*, vol. 49, no. 12, pp. 4771-4787, Dec. 2011.

[3] T. Kræmer, H. Johnsen, and C. Brekke, "Emulating Sentinel-1 Doppler radial ice drift measurements using Envisat ASAR data," *IEEE Trans. Geosci. Remote Sens.*, vol. 53, no. 12, pp. 6407-6418, Dec. 2015.

[4] L. H. Smedsrud, M. H. Halvorsen, J. C. Stroeve, R. Zhang, and K. Kloster, "Fram Strait sea ice export variability and September Arctic sea ice extent over the last 80 years," *Cryosphere*, vol. 11, pp. 65-79, Jan. 2017.

[5] M. W. Hansen, F. Collard, K.-F. Dagestad, J. A. Johannessen, P. Fabry, and B. Chapron, "Retrieval of sea surface range velocities from Envisat ASAR Doppler centroid measurements," *IEEE Trans. Geosci. Remote Sens.*, vol. 49, no. 10, pp. 3582-3592, Oct. 2011.

[6] T. Kræmer, H. Johnsen, C. Brekke, and G. Engen, "Comparing SAR-based short time-lag cross correlation and Doppler-derived sea ice drift velocities," *IEEE Trans. Geosci. Remote Sens.*, vol. 56, no. 4, pp. 1898-1908, Apr. 2018.

[7] A. Korosov and P. Rampal, "A combination of feature tracking and pattern matching with optimal parametrization for sea ice drift retrieval from SAR data," *Remote Sens.*, vol. 9, no. 3, pp. 258, Mar. 2017.

[8] G. Engen and H. Johnsen, "High-precision Doppler frequency estimation for ocean applications," in *Proc. SEASAR*, Tromsø, Norway, 18-22 June 2012, ESA SP-704, pp. 127-130.

[9] I. G. Cumming and F. H. Wong, *Digital Processing of Synthetic Aperture Radar Data: Algorithms and Implementation*, Norwood, MA, USA, Artech House, 2005.

[10] M. V. Dragoševic and R. Ferrara, "Physical characterization and comparison of Doppler and attitude estimates for ENVISAT/ASAR and RADARSAT-1," in *Proc. CEOS SAR Workshop*, Ulm, Germany, 27-28 May 2004.

[11] *Envisat-1 mission CFI software mission conventions document*, document PO-IS-ESA-GS-0561, Issue 2.0, GMV, S.A, Madrid, Spain, 1997. Available: http://eop-cfi.esa.int/Repo/PUBLIC/DOCUMENTATION/CFI/ENVCFI/5.9_Documentation/mcd2.0.pd

[12] A. Recchia, A. Monti Guarnieri, N. Miranda, F. Collard, D. D'Aria, D. Giudici, "Impact of the antenna stability on the Doppler Centroid frequency," in *Proc. IGARSS*, Vancouver, Canada, 24-29 Nov. 2011, pp. 1516-1519.